Irrigation & Drainage Systems Engineering

Research Article Open Access

Pressure Head Profile of Linear-Move Sprinkler Irrigation Laterals: Analysis, Equation and Profile Patterns

Zerihun D[1]* and Sanchez CA[2]

[1]*Maricopa Agricultural Center, University of Arizona, 37860, W. Smith-Enke Rd, Maricopa, Arizona, AZ 85138-3010, USA*
[2]*Department of Soil, Water, and Environmental Science and Maricopa Agricultural Center, University of Arizona, 37860 W. Smith-Enke Rd, Maricopa, Arizona, AZ 85138-3010, USA*

Abstract

An equation that expresses lateral pressure as an explicit function of distance from the lateral inlet is derived for linear-move sprinkler irrigation systems. The equation takes into account the effects of both field slope and span geometry on lateral pressure. The proposed equation is not intended for predictive use. Instead, it is used here in an additional evaluation of the validity of the unique pressure profile variability patterns, of linear-move laterals, produced in an earlier study through numerical simulations. Accordingly, the pressure profiles computed with the equation are compared with those obtained through simulations. Six data-sets, covering a range of field slopes and lateral parameters, are used in the evaluation. The results show that pressure profiles computed with the equation closely match those obtained through simulations. Overall, the spatial patterns of the pressure profiles computed here, with the equation, confirm observations made in an earlier study that the variability attributes of the pressure profiles of linear-move laterals exhibit dual characteristics, consisting of local span-scale variability patterns and inter-span/lateral-wide trends. Analysis of the pressure head equation shows that pressure head profile of a lateral is a stepwise linear function of distance from the inlet with discontinuities at computational nodes. The practical significance of this observation in the computation and description of lateral pressure head profile is highlighted. The pressure head equation derived here is also used to define a pressure slope function that can potentially be used to characterize the full range of variation of the pressure profile patterns of linear-move laterals.

Keywords: Pressure head profile; Friction slope; Lateral slope; Piece-wise linear; Step function; In-span variability; Inter-span trends

Introduction

Hydraulic modeling of continuous-move sprinkler irrigation systems, including linear-move laterals, has been the subject of various studies [1-10]. Equations that express pressure as an explicit function of distance from the lateral inlet were used in computing pressure profiles along irrigation laterals [2,4,7]. Earlier studies considered laterals that are generally composed of straight pipe sections, hence variations in lateral elevation profiles were presumed to be entirely due to the topography of the field that the laterals are installed in. However, because of the curvature of the spans, the elevation profile of a linear-move lateral varies not only with the field slope, but also as a function of the span geometry. Thus, a more accurate determination of the pressure profiles of a linear-move lateral requires taking into account, both span geometry and field slope effects, on lateral elevation profiles.

Accordingly, this paper derives an equation that expresses the pressure along a linear-move lateral as an explicit function of distance from the lateral inlet, accounting for span geometry and field slope effects. To derive the pressure head equation, first the lateral pressure head equation is written in its general form based the energy conservation principle for one-dimensional steady flow in pipes. The spatial behavior of each term of the equation is then analyzed and a function that relates the relevant parameter explicitly with distance from the lateral inlet is defined. Finally, the expressions for each parameter are assembled to form the equation that relates pressure explicitly with distance from the lateral inlet.

The pressure profile equation developed here is not intended for predictive use. In the current study, pressure profiles computed with the explicit pressure-distance equation were used in further evaluation of the validity of the distinct pressure profile patterns, of linear-move laterals, produced earlier through simulations [11]. Accordingly, pressure head profiles computed with the equation were compared with model predictions. Six data-sets covering a range of lateral parameters and field slopes were used in the evaluation. The results show that the pressure profiles produced by the equation and the simulation model are in good agreement, lending additional support to the validity of the rather unique variability patterns of the pressure profiles of linear-move laterals.

Overall, pressure profiles computed with the equation presented here confirm the observation by Zerihun et al. [11] that the pressure profile variability attributes of linear-move laterals show dual characteristics, consisting of local span-scale (in-span) variability patterns and a broader inter-span/lateral wide trend. Specifically, the results show that the pressure head profile of a linear-move lateral is a concatenation of a series of convex, and at times concave, segments punctuated by sharp transition at span boundaries. Convex in-span pressure variability patterns were observed over spans that have a concave form. By comparison, a span with a convex elevation profile has produced a concave in-span pressure variability pattern.

Furthermore, it is shown here that span-scale pressure differentials, when considered over multiple consecutive spans, yield an inter-span/lateral-wide pressure variability trend. The inter-span/lateral-wide pressure variability trend along a lateral is represented here in terms of a relatively simple curve, with distinct monotonic properties, obtained by connecting the pressure heads at the inlet and distal ends of each span. The results show that the inter-span pressure variability trend

***Corresponding author:** Zerihun D, Associate Research Scientist, Maricopa Agricultural Center, University of Arizona, 37860, W. Smith-Enke Rd, Maricopa, AZ 85138-3010, USA, Tel: +15203746221, +15209828797; E-mail: dawit@ag.arizona.edu

Received August 14, 2019; **Accepted** September 13, 2019; **Published** September 20, 2019

Citation: Zerihun D, Sanchez CA (2019) Pressure Head Profile of Linear-Move Sprinkler Irrigation Laterals: Analysis, Equation and Profile Patterns. Irrigat Drainage Sys Eng 8: 239.

curve is able to effectively capture the broader lateral-wide variability attributes of pressure in a manner that is readily discernible and hence suitable for comparison and analysis of alternative hydraulic scenarios.

The pressure head equation is also used to define a function that relates pressure slope with lateral slope and friction slope along a linear-move lateral. Following the approach used by Martin et al. [12] and Zerihun et al. [13], the pressure slope equation can be used in the analysis and characterization of the full range of variation of the pressure profile patterns of linear-move laterals. However, the current study is limited to highlighting some important properties of the pressure slope equation.

Analysis of the spatial behaviors of key lateral hydraulic parameters and lateral elevation profile, conducted here in the course of the development of the pressure profile equation, has led to interesting observations on the mathematical properties of the parameters and the lateral pressure profile itself. An important result in this regard relates to an observation that the pressure head profile of an irrigation lateral is a piecewise linear function of distance from the lateral inlet with discontinuities at the computational nodes. The practical implication of this result is that a more complete description of the pressure profile of a lateral needs to take the form of an array in which pressure about each computational node is defined in terms of a pair of values, consisting of a pressure head at a point just upstream and another one at a point just downstream of the node. Note that this characterization does not apply to the inlet- and distal-end nodes of a lateral. For each of these nodes pressure can be defined in terms of a single value.

Analysis and Development of the Lateral Pressure Profile Equation

An equation that expresses lateral pressure as an explicit function of distance from the lateral inlet would be derived here for a linear-move sprinkler irrigation lateral with or without pressure reducing valves (*prvs*).

Description of terms

Development of the pressure head profile equation assumes that, over a lateral pipe segment, the lateral hydraulic and geometric characteristics as well as the slope of the lateral centerline are invariant with distance from the lateral inlet. A lateral pipe segment is defined here as a line spanning two consecutive computational nodes of a lateral. The term computational nodes, or simply nodes, refers to points representing the lateral inlet, lateral outlet ports, span joints, and the distal-end of the lateral in the schematization of a sprinkler irrigation lateral for computational purposes [10]. Lateral outlet ports and span joints are also described in this paper as junction nodes, because they represent points where two or more hydraulic links are joined. A hydraulic link can be a lateral pipe segment, a droptube-sprinkler assembly, or a droptube-*prv*-sprinkler assembly. Note that in the context of the current study a *prv* is a pressure reducing valve installed at the inlet end of a sprinkler to regulate sprinkler inlet pressure at a pre-set level.

The horizontal distance between a pair of consecutive computational nodes (i.e., the length of the projection on the horizontal axis of a lateral pipe segment) is an important parameter in the pressure equation that will be derived subsequently. Given the geometry of linear-move spans, this distance is typically different from the length of the corresponding lateral pipe segment. Thus, in subsequent developments the horizontal distance between two consecutive computational nodes will be referred to as the nodal interval.

Lateral pressure head profile equation

Assuming flow along a linear-move lateral is one-dimensional and steady, it can be observed from Figure 1 that the energy balance equation between the lateral inlet and any point located at distance x from the lateral inlet can be expressed as

$$H_0 = H(x) + H_f(x) + H_l(x) \quad (1)$$

In Eqn. 1, H_0 is the total head at the lateral inlet *[L]*; *H(x)* is the total head at distance x from the inlet *[L]*; and $H_f(x)$ and $H_l(x)$ are, respectively, the friction and local head losses over distance x from the inlet *[L]*. Expressing *H(x)*, in Eqn. 1, in terms of its components shown in Figure 1 yields

$$H_0 = Z(x) + h(x) + V_h(x) + H_f(x) + H_l(x) \quad (2)$$

In Eqn. 2, *Z(x)* is elevation of the lateral centerline at distance x from the lateral inlet *[L]*; and *h(x)* and $V_h(x)$ are, respectively, the lateral pressure head and the velocity head at distance x from the inlet *[L]*. The

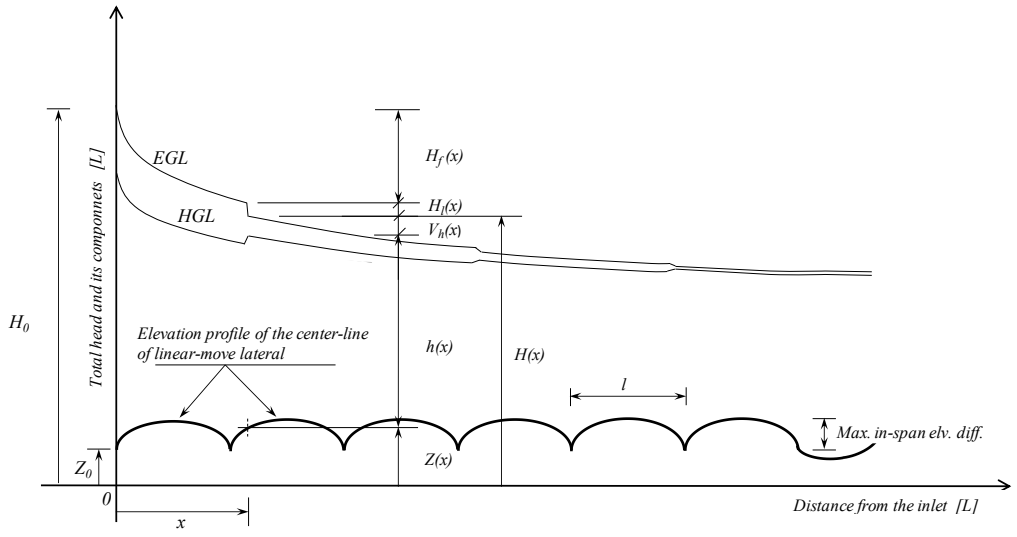

Figure 1: Schematics of the components of water specific energy along a linear move lateral (where: *EGL* is energy grade line and *HGL* is hydraulic grade line).

pressure head at distance x from the inlet, $h(x)$, can then be expressed as

$$h(x) = H_0 - H_f(x) - H_l(x) - V_h(x) - Z(x) \quad (3)$$

Eqn. 3 is a general expression of lateral pressure head profile in irrigation laterals. Overall, the pressure head profiles of linear-move laterals are functions of the hydraulic (total head at the inlet, pipe surface roughness, and sprinkler and *prv* hydraulic characteristics), geometric (pipe diameter, nodal interval, and lateral length), and elevation characteristics (span curvature parameters, span length, and field slope) of the lateral. However, it needs to be pointed out here that the effects of most of the lateral hydraulic and geometric parameters on lateral pressure head profiles, $h(x)$, are not explicitly taken into account in Eqn. 3, instead they are implicitly expressed in terms of the $H_f(x)$, $H_l(x)$, $V_h(x)$, and $Z(x)$ profiles.

Considering that the inlet head, H_0, and the lateral elevation profile, $Z(x)$, are known constants, it can be observed that Eqn. 3 can produce an accurate estimate of lateral pressure, provided the $H_f(x)$, $H_l(x)$, and $V_h(x)$ terms are evaluated through hydraulic simulations in which continuity and energy balance requirements for steady flow in pipes are satisfied. It is, thus, presumed here that the $H_f(x)$, $H_l(x)$, and $V_h(x)$ terms in Eqn. 3 are obtained through such simulations. Accordingly, friction head losses and velocity heads are generally defined over a finite number of lateral pipe segments and local head losses are specified at discrete points (i.e., computational nodes) along the lateral. Note that the notations $H_f(x)$, $H_l(x)$, $V_h(x)$, and $Z(x)$ are used here to refer, in a more general sense, to the profiles of the respective parameters along the lateral. Alternatively, they are also used to reference the specific value of the parameters at some distance x from the lateral inlet.

Analysis of parameter variability with distance from the lateral inlet

The development of a (linear-move) lateral pressure profile equation, that expresses pressure as an explicit function of distance from the lateral inlet, will now be presented in two main steps. First, the behavior of each term of Eqn. 3 is analyzed and a function that relates the relevant parameter explicitly with distance from the lateral inlet is defined. Then the expressions for each parameter are assembled to form the equation that relates pressure explicitly with distance from the lateral inlet.

Friction head loss: Given that lateral discharge shows a step change across a node representing a lateral outlet, it can be readily observed that (within the framework of a one-dimensional steady flow formulation of lateral hydraulics) the friction head loss profile of an irrigation lateral, $H_f(x)$, is a monotonic increasing, piecewise linear, function of distance (Figure 2a). It is linear over a nodal interval, but generally has different slopes across a node. However, friction head loss can have the same slope across span joints, i.e., nodes with zero outflow discharge. Note that such nodes typically account for a tiny fraction, less than about 0.1%, of the number of computational nodes along a linear-move lateral.

It can be observed from the preceding characterization of $H_f(x)$ that the slope of the $H_f(x)$ profile, referred here simply as friction slope, is constant over a nodal interval. Thus, the friction slope over any given nodal interval, say over the interval spanning the *(q-1)th* and the *qth* nodes (Figures 2a and 2b), can be given as

$$\left.\begin{aligned} H'_{f,q} &= \frac{H_f(x_q) - H_f(x_{(q-1)})}{\Delta x_q}, \qquad for\ 1 \le q \le Q \\ where \quad \Delta x_q &= x_q - x_{(q-1)} \quad and \quad x_{(q-1)} = \sum_{i=1}^{(q-1)} \Delta x_i \end{aligned}\right\} \quad (4)$$

As can be noted from Figures 2a and 2b, $H'_{f,q}$ *[-]* is the friction slope over a nodal interval spanning the *(q-1)th* and *qth* nodes; *(q-1)* and *q* are, respectively, indices of the upstream and downstream end nodes delimiting the nodal interval of interest (i.e., the interval over which friction slope is to be determined); x_q is the horizontal distance from the lateral inlet of the *qth* node; and $H_f(x_q)$ is the friction head loss between the lateral inlet and the *qth* node. Furthermore, it can be observed from Figure 2a that *i* is the computational node index and varies between $i = 0$ at the inlet-end and increases along the lateral to *Q* at the distal-end. A closer look at Figure 2a also shows that the index of a nodal interval is equal to the index of the computational node delimiting the downstream end of the nodal interval. Hence, Δx_q, as shown in Eqn. 4, is the nodal interval between the *(q-1)th* and the *qth* nodes. Note that, in Eqn. 4, friction slope is defined with respect to the horizontal axis, not in reference to the centerline of the lateral.

Some important properties of the $H'_f(x)$ profile will now be highlighted. Given that $H_f(x)$ is an increasing function of distance over the entire length of a lateral, it can be readily observed that friction slope, $H'_f(x)$, has positive algebraic sign (i.e., $H'_f(x) > 0$) along a lateral (Note that the usage of the term friction slope in this paper is slightly different from the conventional use of the term, which refers to the slope of the energy line and hence it has a negative algebraic sign). Furthermore, the fact that friction slope, $H'_f(x)$, is constant over a nodal interval (Eqn. 4), but generally varies from one nodal interval to another, implies that it is a step function of distance from the lateral inlet as shown in Figure 2a. However, friction slope can be constant over pair of nodal intervals straddling a node representing a span joint, provided lateral diameter and pipe hydraulic resistance do not change across such a node. Note that the sketch of the $H'_f(x)$ profile shown in Figure 2a considers a lateral with spatially invariant parameter set. However, it needs to be pointed out here that this is meant only to simplify presentation and hence it has no bearing on the scope of applicability of Eqn. 4. In other words, Eqn. 4 is equally applicable to laterals with spatially variable as well as invariant parameter sets.

Based on Eqn. 4, the friction head loss, $H_f(x)$, at a point located at distance x from the inlet, where $x_{(q-1)} < x < x_q$ (Figures 2a and 2b), can now be expressed as the sum of the friction head loss that occurred upstream of the *(q-1)th* node and the incremental change in H_f over δx.

$$H_f(x) = \sum_{i=1}^{(q-1)} \Delta H_{f,i} + H'_{f,q}\delta x, \qquad for\ \ x_{(q-1)} < x < x_q \ \text{ and } \ 1 \le q \le Q \quad (5)$$

Where δx, as shown in Figure 2b, can be given as

$$\delta x = x - \sum_{i=1}^{(q-1)} \Delta x_i, \qquad for\ \ 0 < \delta x < \Delta x_q \quad (6)$$

In Eqn. 5, $\Delta H_{f,i}$ *[L]* is the incremental change in friction head loss over the nodal intervals spanning the *(i-1)th* and *ith* nodes and $H'_{f,q}$ *[-]* is defined in Eqn. 4. Note that $\Delta H_{f,i}$ can be evaluated with an expression of the form, given in the numerator of Eqn. 4, adapted for the *ith* nodal interval.

Based on Eqn. 6, the friction head loss profile, $H_f(x)$, can now be expressed as an explicit function of distance from the lateral inlet, x.

$$H_f(x) = \sum_{i=1}^{(q-1)} \Delta H_{f,i} - H'_{f,q} \sum_{i=1}^{(q-1)} \Delta x_i + H'_{f,q} x, \qquad for\ \ x_{(q-1)} < x < x_q \ \text{ and } \ 1 \le q \le Q \quad (7)$$

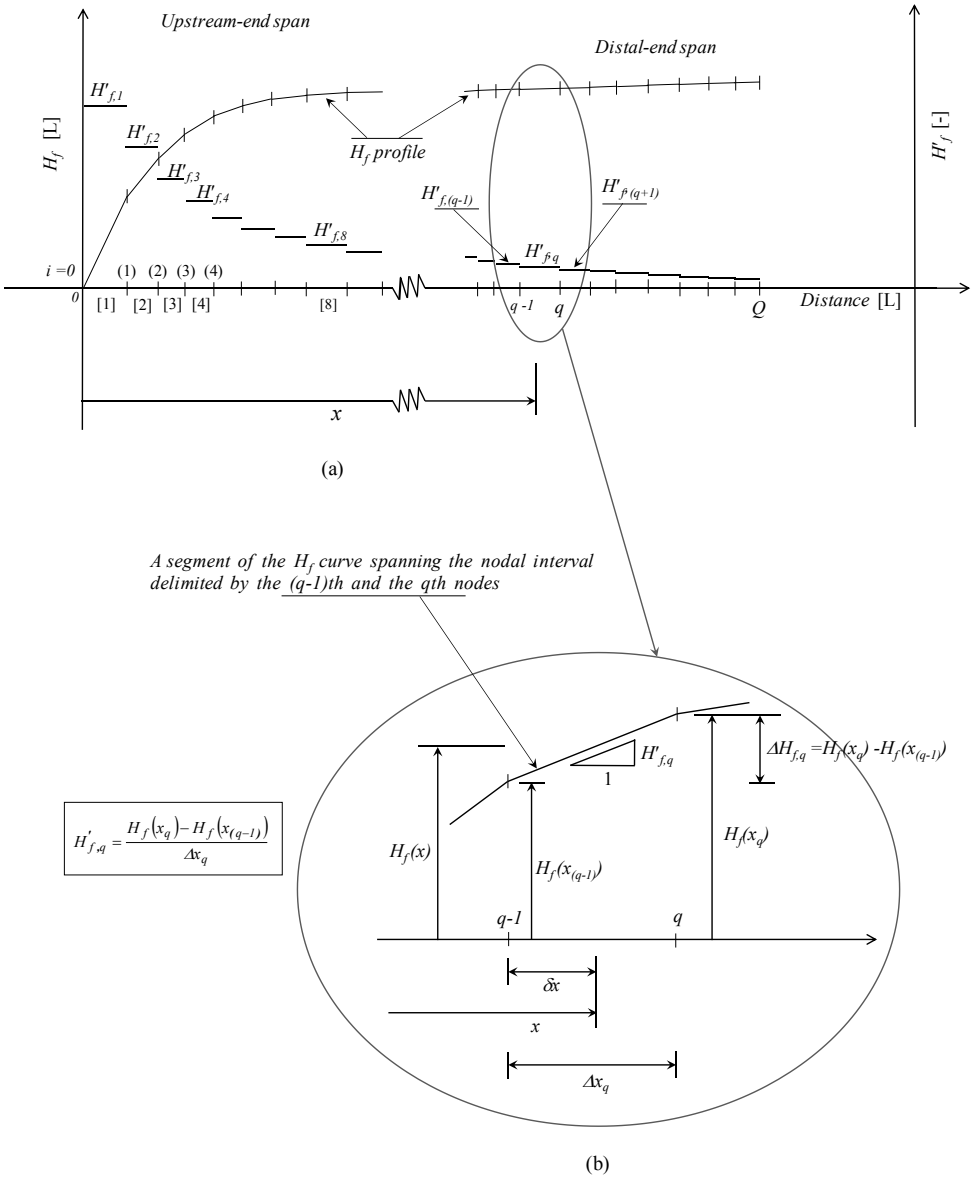

Figure 2: Sketches of: (a) The lateral friction head loss profile, $H_f(x)$, and the friction slope profile, $H_f'(x)$, along a linear-move lateral and (b) A segment of the friction head loss profile spanning the nodal interval $x_{(q-1)}<x<x_q$ (Note: in Figure 2a (.) is computational node index and [.] is nodal interval index).

In Eqn. 7, the first term on the right-hand side is the friction head loss over the lateral section upstream of the *(q-1)th* node. The algebraic sum of the second and third terms represent the incremental change in friction head loss over δx. Note that the first and second terms of Eqn. 7 are constants, but the third term varies as a function of x.

For any given nodal index, q, Eqn. 7 shows that the distance of the point at which friction head loss is to be evaluated, x, varies in the open interval $x_{(q-1)} < x < x_q$, which implies that both $H_f(x)$ and $H_f'(x)$ cannot be evaluated at $x = x_{(q-1)}$ and $x = x_q$. Note that in order to account for the continuity properties of $H_f(x)$ and $H_f'(x)$, a nodal interval will be treated as an open interval in all subsequent discussions.

The significance of Eqn. 7, in the context of the current development, stems entirely from the consideration that it defines the $H_f(x)$ profile in a form that can be used in the derivation of an $h(x)$ equation that relates lateral pressure, h, explicitly with distance from the lateral inlet, x. As will be shown shortly, the pressure profile of an irrigation lateral, $h(x)$, itself shows discontinuity at the nodes. The implication is that the lack of continuity at computational nodes, by the $H_f(x)$ function, imposes no limitations on the accuracy and scope of applicability of the resultant $h(x)$ equation and hence on the practical significance of Eqn. 7 in the context of the current application. Note that Eqn. 7 can be used to obtain an accurate estimate of $H_f(x_{(q-1)})$ and $H_f(x_q)$ by setting x sufficiently close to $x = x_{(q-1)}$ and $x = x_q$, respectively.

Local head loss: Local head losses that are of interest here are those associated with flow division that occurs across lateral nodes. Although these losses have two components, the local head loss term that is relevant to the determination of the pressure profile of a lateral with Eqn. 3 is the loss component associated with the through-flow across

junction nodes. Thus, the local head loss, $H_l(x)$, between the lateral inlet and any given point along the lateral, say a point located at distance x from the lateral inlet (where $x_{(q-1)} < x < x_q$), can be given as

$$H_l(x) = \sum_{i=1}^{(q-1)} \Delta H_{l,i}, \qquad for \quad x_{(q-1)} < x < x_q \tag{8}$$

In Eqn. 8, $\Delta H_{l,i}$ *[L]* is the local head loss that occurs across the *ith* node along the lateral. Note that Eqn. 8 defines $H_l(x)$, where $x_{(q-1)} < x < x_q$, as the sum total of the local head losses that occurred at and upstream of the *(q-1)th* node. Note that Eqn. 8 defines $H_l(x)$ as a step function of distance (Figures 3a and 3b). Thus, $H_l(x)$ is constant over a nodal interval, but increases across each node.

Lateral elevation profile: The elevation profile of a linear-move lateral is comprised of a series of curves representing the centerlines of the arched spans, each with a concave or convex form (Figures 1 and 4a). The elevation profiles of each span can be modeled accurately with a second- or third-order function [11]. Thus, the slope of the centerline of each span vary continuously with distance from the lateral inlet and can be calculated directly with the derivatives of the $Z(x)$ functions of the spans. However, based on practical computational considerations, lateral pipe segments are treated here as hydraulic links, instead of the actual (curved) lateral pipe sections connecting any two consecutive computational nodes. The implication is that given a nodal interval, the corresponding lateral slope is defined as the slope of the lateral pipe segment spanning the interval. As shown in Figure 4b, the elevation

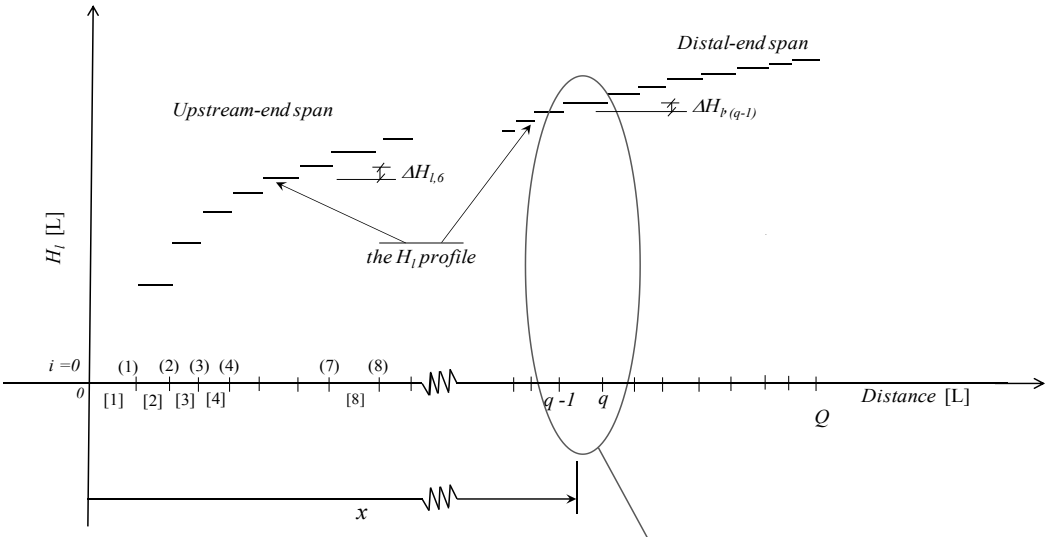

Figure 3: Sketches showing: (a) Variations in the nodal local head loss, $\Delta H_{l,i}$, and the corresponding local head loss profile, H_l(x), along a linear-move lateral and (b) A segment of the H_l(x) profile spanning the nodal interval $x_{(q-1)} < x < x_q$ (Note: in Figure 3a, (.) is computational node index and [.] is nodal interval index).

profile of a lateral pipe segment is an approximation of the actual lateral pipe section profile. Because of the low curvature of linear-move spans and the relatively small outlet spacing this approximation is generally accurate.

Accordingly, the constant lateral slope over any given nodal interval, say the interval spanning the *(q-1)th* and the *qth* nodes (Figures 4a and 4b), labeled here as Z'_q can be given as

$$Z'_q = \frac{Z(x_q) - Z(x_{q-1})}{\Delta x_q}, \qquad for \quad 1 \le q \le Q \tag{9}$$

Note that because of the approximation introduced in the determination of lateral slope (Figures 4a and 4b), the lateral slope profile, *Z'(x),* is a step function of distance from the lateral inlet and hence it is not continuous at the computational nodes.

Some of the characteristic features of the *Z'(x)* profile of both concave and convex spans of linear-move systems are summarized here. As can be noted from Figure 4a, the *Z'(x)* function of a concave span is a decreasing step function of distance from the lateral inlet. It has an upstream section with a positive *Z'(x)* profile and a downstream section with a negative *Z'(x)* profile. In addition, the spatial variability pattern of the *Z'(x)* profile is repeated from one span to the next, provided the spans are of exactly the same geometry and are installed over a field with a constant slope. Although the *Z'(x)* profile of a span with a convex form is not depicted in Figure 4a, it can be readily reasoned that it would have the following characteristics: it would be an increasing, step function, of distance from the lateral inlet with an upstream section where the *Z'(x)* profile is negative and a downstream section in which the *Z'(x)* profile is positive. Unlike the concave spans,

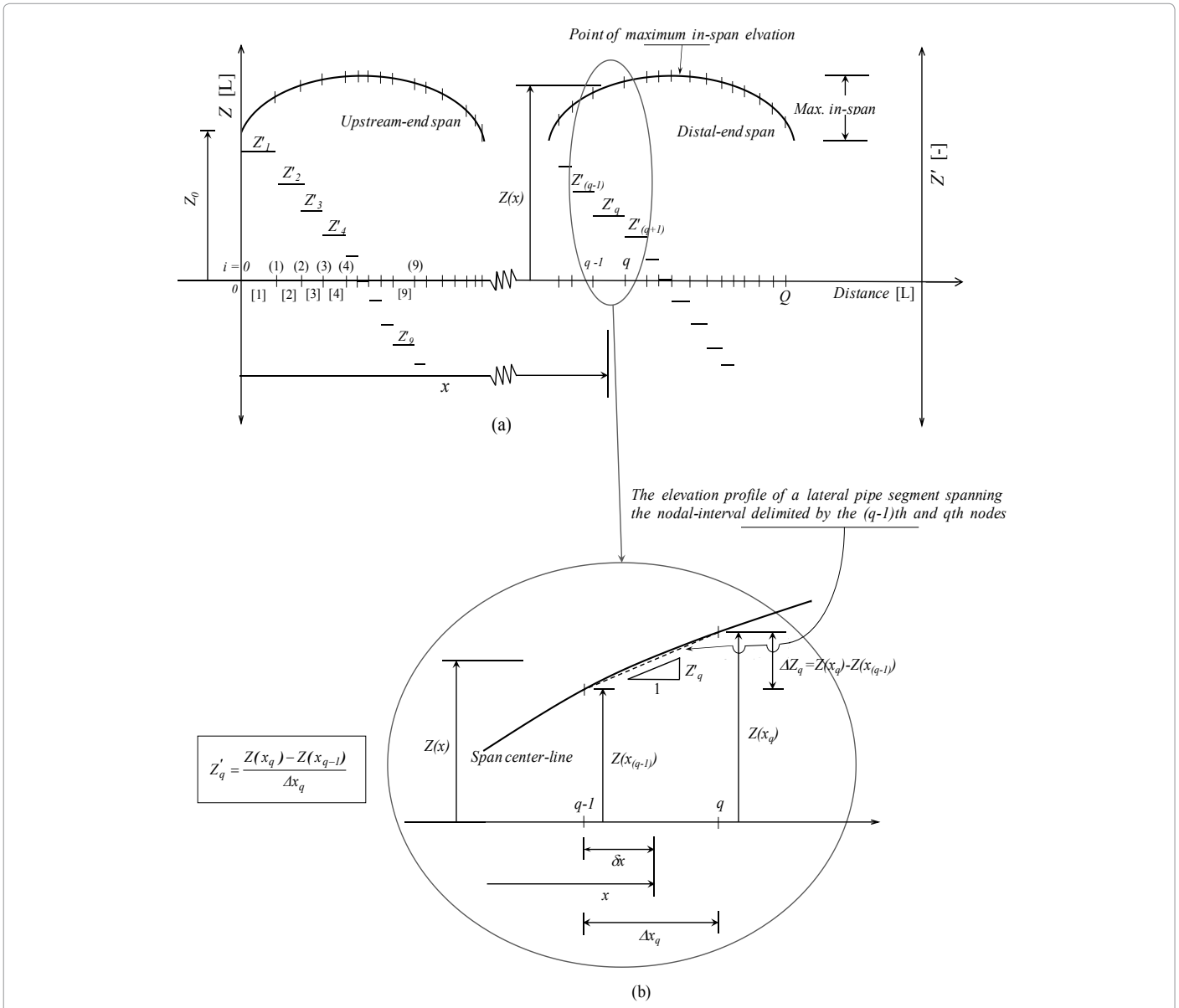

$$Z'_q = \frac{Z(x_q) - Z(x_{q-1})}{\Delta x_q}$$

Figure 4: Sketches of: (a) The lateral elevation profile, *Z(x)*, and the lateral slope profile, *Z'(x)*, along a linear-move lateral and (b) The elevation profile of a lateral pipe segment spanning the nodal interval $x_{(q-1)} < x < x_q$ (Note: in Figure 4a, (.) is computational node index and [.] is nodal interval index).

the *Z'(x)* profile of a convex span is not repeated along the lateral, because linear-move laterals typically have only one span with a convex form located at their distal-ends.

Eqn. 9 can now be used to formulate an expression for the lateral elevation profile, *Z(x)*, as the algebraic sum of the elevation of the lateral inlet and the net incremental change in lateral elevation, from the inlet, over distance *x*.

$$Z(x) = Z_0 + \left(\sum_{i=1}^{(q-1)} \Delta Z_i + Z_q' \delta x \right), \quad for \quad x_{(q-1)} < x < x_q \quad and \quad 1 \le q \le Q \tag{10}$$

In Eqn. 10, Z_0 is the elevation of the lateral inlet *[L]*, which is a given constant, and ΔZ_i *[L]* is the elevation differential over the nodal interval spanning the *(i-1)th* and the *ith* nodes (e.g., Figure 3b). Note that the parenthetical expression in Eqn. 10 is the net incremental change in lateral elevation, over distance *x* from the lateral inlet, with respect to the elevation of the lateral inlet, Z_0.

Using Eqn. 6 in Eqn. 10, the lateral elevation profile can now be expressed as a function of distance from the lateral inlet

$$Z(x) = \left(Z_0 + \sum_{i=1}^{(q-1)} \Delta Z_i \right) - Z_q' \sum_{i=1}^{(q-1)} \Delta x_i + Z_q' x, \quad for \quad x_{(q-1)} < x < x_q \quad and \quad 1 \le q \le Q \tag{11}$$

The expression in parenthesis, on the right-hand side of Eqn. 11, represents the lateral elevation at the *(q-1)th* node. The algebraic sum of the second and third terms on the right-hand-side is the incremental change in lateral elevation over δx (Figure 4b).

Note that according to the formulation presented in Eqn. 11, *Z(x)* is not continuous at the computational nodes, which evidently is related to the continuity property of the *Z'(x)* function (Eqn. 9). As will be shown shortly, the *h(x)* function itself is not defined at computational nodes. Thus, the lack of continuity at nodal points, by the *Z(x)* function, should not impose limitations on the accuracy and scope of applicability of the resultant *h(x)* equation and hence on the practical significance of Eqn. 11 in the context of the current application. Note that Eqn. 11 can be used to obtain an accurate estimate of $Z(x_{(q-1)})$ and $Z(x_q)$ by taking *x* sufficiently close to $x = x_{(q-1)}$ and $x = x_q$, respectively.

Lateral inlet head and velocity head: As noted earlier, lateral inlet head, H_0, is considered a given constant. The velocity head profile, $V_h(x)$, on the other hand, has similar spatial variability characteristics as friction slope profile. It is discontinuous across outlet nodes and is a step function of distance from the lateral inlet (Figure 5a). As can be noted from Figure 5b, the $V_h(x)$ profile can thus be expressed as:

$$h'(x) = -H_{f,q}' - Z_q', \; for \; x_{(q-1)} < x < x_q \; and \; 1 \le q \le Q \tag{12}$$

In Eqn. 12, $V_{h,q}$ is the velocity head over a nodal interval spanning the *(q-1)th* and the *qth* nodes *[L]*. Note that the velocity head profile, shown in Figure 5a, considers a lateral with constant diameter over its entire length. However, it ought to be noted that this is meant only to simplify presentation and hence it has no bearing on the scope of applicability of Eqn. 12 and the pressure head equation that is being developed.

Equation that relates lateral pressure explicitly with distance from the lateral inlet: Substituting the expressions for $H_f(x)$, $H_l(x)$, *Z(x)*, and $V_h(x)$, given in Eqns. 7, 8, 11, and 12, in the pressure head profile equation, Eqn. 3, yields a function that expresses lateral pressure, *h(x)*, as an explicit function of distance from the lateral inlet, *x*.

$$h(x) = \left(H_0 - Z_0\right) - \left(\begin{array}{l} \sum_{i=1}^{(q-1)} \Delta H_{f,i} + \sum_{i=1}^{(q-1)} \Delta Z_i - \left(H_{f,q}' + Z_q' \right) \\ \sum_{i=1}^{(q-1)} \Delta x_i + \sum_{i=1}^{(q-1)} \Delta H_{l,i} + V_{h,q} \end{array} \right) - H_{f,q}' x - Z_q' x, \; for \; x_{(q-1)} < x < x_q \; and \; 1 \le q \le Q \tag{13}$$

In Eqn. 13, the first and second parenthetical terms as well as the coefficients of the third and fourth terms, on the right hand side of the equation, are known constants given the distance from the lateral inlet, *x*. They are given inputs (such as H_0 and Z_0) or calculated from the inputs (ΔZ_i, Δx_i, $\Delta Z'_q$, $H_{f,i}$, $H'_{f,q}$, ΔH_{Pi} and $V_{h,q}$). However, the third and fourth terms vary with distance, *x*.

A closer look at Eqn. 13 and the continuity properties of the $H'_f(x)$ and *Z'(x)* functions, described earlier, reveals some important properties of the lateral pressure head profile, *h(x)*. It shows that the *h(x)* profile exhibits a linear trend and is continuous over a nodal interval, but is discontinuous at computational nodes. The pressure profile of a lateral can thus be described as a piecewise linear function of distance from the lateral inlet. Further discussion on the practical significance of this observation will be presented shortly.

Equation 13 represents a general expression that relates lateral pressure head with inlet boundary conditions, friction and local head losses, velocity head, and lateral elevation profile and as such it can be applied not only to linear-move laterals, but also to laterals of solid-set and set-move sprinkler irrigation systems. As noted earlier, some of the inputs to Eqn. 13 are outputs of hydraulic simulations, which implies that the *h(x)* profile computed with Eqn. 13 is in fact a redundant information in so far as pressure prediction is concerned, because the same profile would have already been determined with the simulation conducted prior to the evaluation of the equation. This shows that Eqn. 13 is not designed for predictive use and hence cannot be used as a substitute for hydraulic simulations. The significance of Eqn. 13, however, lies mainly in its directness and relative simplicity in representing lateral pressure as an explicit function of distance from the lateral inlet.

Because of the relative simplicity of Eqn. 13, it can be reasoned that results of comparisons of pressure profiles computed with Eqn. 13 and a numerical hydraulic model [11] can be part of a more comprehensive evaluation package designed to assess the validity of the unique pressure profile patterns of linear-move laterals. Given that Eqn. 13 expresses pressure as an explicit function of distance from the lateral inlet, it can also be useful in the analysis and characterization of the full range of variation of the pressure profile patterns of linear-move laterals. Furthermore, analysis of the spatial behaviors of key lateral hydraulic parameters and lateral elevation profile characteristics, conducted here as part of the derivation of Eqn. 13, has revealed some interesting properties of the parameters. In the following section, applications of the explicit pressure-distance equation will be elaborated further and a summary of the spatial behaviors of important lateral hydraulic parameters will be presented.

Applications of the Pressure Head Profile Equation and Summary of the Spatial Behaviour of Pertinent Parameters

Assessment of the validity of the distinct pressure profile patterns of linear-move laterals predicted by numerical models: Lateral pressure profiles computed with Eqn. 13 can be used in assessing

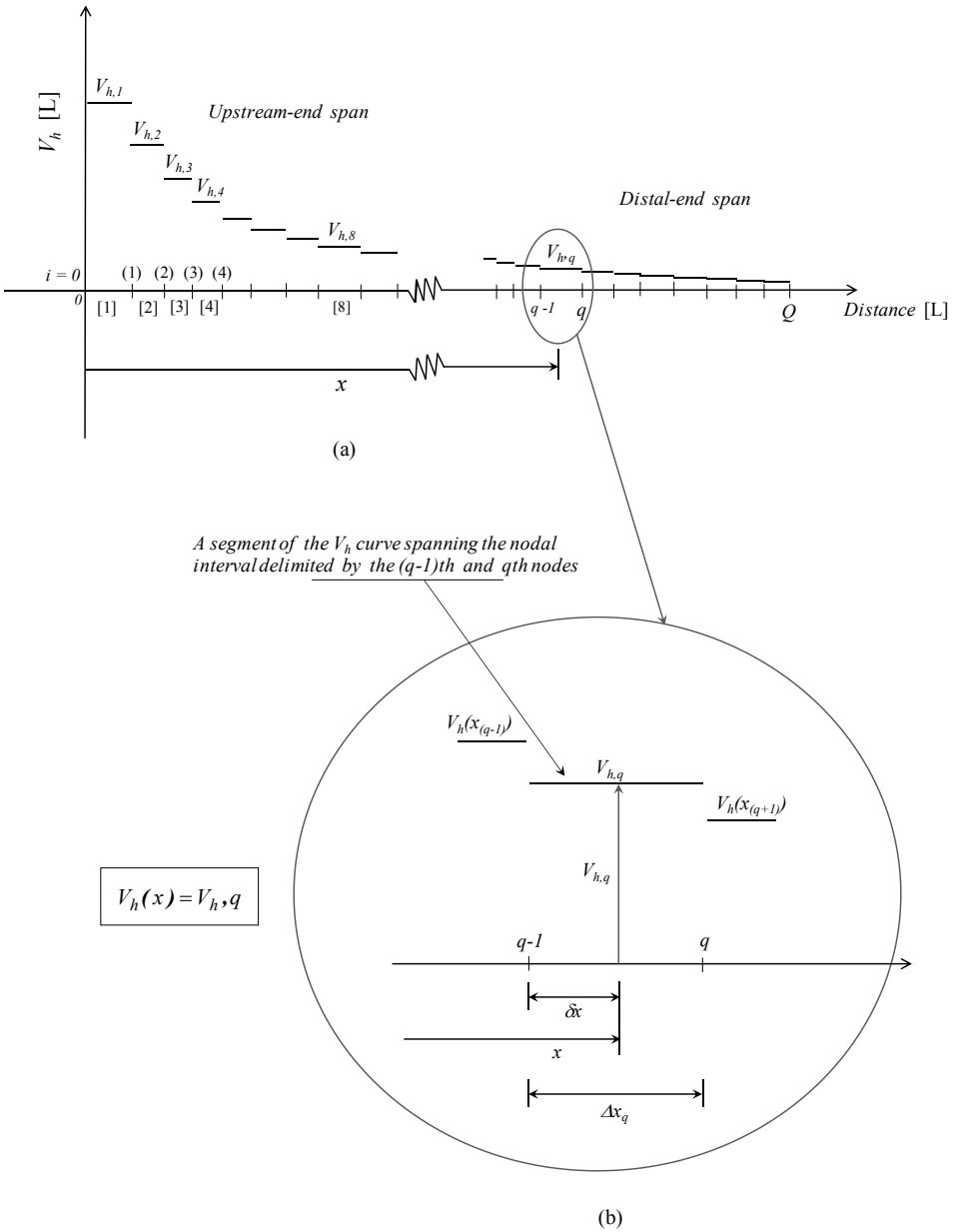

Figure 5: Sketches of: (a) The velocity head profile, $V_h(x)$, along a linear-move lateral and (b) A segment of the $V_h(x)$ profile spanning the nodal interval $x_{(q-1)} < x < x_q$. (Note: in Figure 5a, (.) is computational node index and [.] is nodal interval index).

the validity of the pressure profile patterns, of linear-move laterals, predicted by numerical models. As noted earlier, pressure profiles computed with Eqn. 13 do not represent completely independent predictions from those obtained through simulations. Nonetheless, a close agreement between the pressure predictions of Eqn. 13 and a numerical hydraulic model would lend additional support to the validity of the distinct pressure profile patterns of linear-move laterals computed with the model. On the other hand, a lack of satisfactory agreement between lateral pressure profile estimates obtained with the equation and the model would point to potential inaccuracies in the model and would raise questions regarding the validity of the distinct pressure profile patterns of linear-move laterals computed with the model. Accordingly, the explicit pressure-distance equation derived here will be used here in an additional evaluation of the pressure profile patterns, of linear-move laterals, produced by the hydraulic simulation model proposed by Zerihun et al. [11].

Pressure slope equation: A pressure slope equation, for a linear-move lateral, can be a valuable tool in characterizing the full range of variation of lateral pressure head profile patterns [13,14]. Such an equation will be defined here based on Eqn. 13 and it is key properties will be highlighted. However, analysis of linear-move lateral pressure profiles using this equation is outside the scope of the current study and will have to await a follow up study.

Accordingly, the pressure slope at any given point in a nodal interval, say at a point located at distance x from the lateral inlet (where $x_{(q-1)} < x < x_q$), can be calculated with Eqn. 14.

$$h'(x) = -H'_{f,q} - Z'_q, \text{ for } x_{(q-1)} < x < x_q \text{ and } 1 \le q \le Q \quad (14)$$

In Eqn. 14, $h'(x)$ is the pressure slope at distance x from the lateral inlet *[-]*. Note that Eqn. 14 is obtained by differentiating the $h(x)$ equation, Eqn. 13, over a nodal interval with respect to distance from the lateral inlet, x. Since both the friction slope, $H'_{f,q}$, and the lateral slope, Z'_q, are step functions of distance from the lateral inlet, it can be observed that the pressure slope profile, $h'(x)$, as well is a step function of distance and is defined over the nodal intervals, but not at the nodes delimiting the intervals. Note that this property of the $h'(x)$ function can also be inferred directly from the spatial behavior of the pressure head profile, $h(x)$, discussed earlier in relation to Eqn. 13.

Given the hydraulic, geometric, and elevation profile characteristics of a lateral, Eqn. 14 shows that the pressure slope profile, $h'(x)$, and hence the spatial variability pattern of the corresponding pressure profile of a linear-move lateral, or any other lateral for that matter, is dependent only on the interactive effects of the lateral slope and the friction slope profiles. The pressure slope is independent of the boundary condition constants, i.e., H_0 and Z_0. It is also independent of the velocity head profile, $V_h(x)$, and the local head loss profile, $H_l(x)$. While the velocity head, $V_h(x)$, and local head loss, $H_l(x)$, profiles have some effect on $h(x)$, the fact that both $V_h(x)$ and $H_l(x)$ are invariant with distance over a nodal interval meant that they have no effect on the pressure slope over the same interval. The preceding observations imply that two different irrigation scenarios can have the same pressure slope profile and hence lateral pressure head profile pattern, if only they have the same friction slope and lateral slope profiles.

The spatial behavior of lateral hydraulic parameters and elevation profile characteristics: Analysis of the spatial behaviors of some of the key lateral hydraulic parameters and lateral elevation profile characteristics, conducted here in the course of the development of the pressure head equation, has revealed some interesting mathematical properties of the parameters and lateral pressure profile itself. These properties are highlighted here.

It is observed that the friction head loss profile is a piecewise linear function, and the velocity head profile is a step function, of distance from the lateral inlet. Both profiles show discontinuities at computational nodes representing outlet ports. It is also shown here that the local head loss profile can be represented as a step function of distance from the lateral inlet. The slope of the local head loss and velocity head profiles, both of which are defined over a nodal interval, are therefore zero. Furthermore, lateral elevation profile is defined here as a piecewise linear function of distance from the lateral inlet. Hence, the slopes of the lateral elevation as well as the friction head loss profiles are step functions of distance.

Based on these observations and Eqn. 13, it is deduced here that the pressure head profile of a lateral is a piecewise linear function of distance from the lateral inlet with discontinuities at the computational nodes and hence the pressure slope profile is a step function of distance. The spatial property of lateral pressure head profiles has some practical significance in regard to the computation and description of pressure along a lateral.

The fact that lateral pressure profiles, $h(x)$, are discontinuous at computational nodes implies that pressure can be evaluated about computational nodes, but not at the computational nodes. Thus, in practical numerical computations, involving one-dimensional steady flow, lateral pressures are evaluated at points just upstream and downstream of a computational node. The implication is that a formal and more complete description of lateral pressure profile should take the form of an array in which pressure about each node is defined in terms of a pair of values, consisting of pressure evaluated at a point just upstream and another one at a point just down-stream of the node. These requirement, evidently, does not apply to the inlet-end and distal-end nodes. For these nodes pressure is defined in terms of a single value, computed at a point just downstream and just upstream of the inlet- and distal-end nodes, respectively.

Comparison of Lateral Pressure Profiles Computed With the Equation and Those Obtained Through Simulations

A comparison of the pressure profiles computed with Eqn. 13 and those obtained through hydraulic simulations is presented here. As noted earlier, the goal here is to conduct further evaluation of the validity of the unique spatial variability attributes of the pressure profiles of linear-move laterals obtained, in an earlier study, through simulations. Hydraulic simulations are conducted in this study with model developed by Zerihun and Sanchez [10]. A total of six data-sets were used in the evaluation (Tables 1 and 2). Data-sets 1 to 4 consist of hypothetical laterals and data-sets 5 and 6 are based on irrigation events involving an actual linear-move system described by Zerihun et al. [11]. Description of the data-sets and results of the evaluation will now be presented.

Data description

Note that in subsequent discussion, spans of a lateral are numbered sequentially starting from the upstream-end span, which is referred here as span 1, and increasing in the downstream direction along the lateral.

Data-set 1: Data-set 1 considers a linear-move lateral with six full spans, each 61.25 m long. All spans of the lateral are supported at both ends and are installed on a level field (Tables 1 and 2). The total head at the lateral inlet, H_0, is set to 30 m. The lateral inlet elevation, Z_0, with respect to an assumed reference datum, which is the field surface, is 3.8 m. The curves representing the centerlines of all spans of the lateral have identical geometry. The centerline of each span has a concave form and it exhibits symmetry about a vertical line through the point of maximum in-span elevation, when the span is placed on a level surface. In other words, if the lateral is installed in a level field, then the lateral slope is positive over the upper half and is negative over the lower half of each span. The maximum elevation differential within each of these spans is 1.2 m and is the same as the total rise or the total fall in the in-span elevation. Note that the elevation profile of these spans was modeled with the equation of a circle.

Lateral diameter of 127 mm is used over the entire length of the lateral and the pipe absolute roughness is 0.005 mm (Table 1). Outlets are spaced at a regular horizontal interval of 1.25 m along the lateral. Water is conveyed from each outlet down to a *prv*-sprinkler assembly with a drop-tube. Drop-tube lengths, which vary between 3.05 and 4.25 m, are set such that the sprinkler-*prv* assembly is suspended from the laterals at a constant above ground clearance of 0.75 m along the lateral, if the lateral was to be operated in a level field. The absolute roughness and the diameter of the drop-tubes used in the lateral are 0.0015 and 19.05 mm (Table 1), respectively.

The sprinkler model considered here is Supper spray UP3 produced by Senniger [15] and it has a nozzle diameter of 3.572 mm (9/64″). The parameters of the sprinkler head-discharge function, derived based on data provided in the manufacturer's catalogue, are summarized

Lateral parameters		**Units**	**Data-set**				
			1[a]	**2**	**3**	**4**	**5 and 6**
Number of spans		-			6		7
Span geometry	Concave				6		6
	Convex				-		1
Effective span length		m			61.25		27, 50.8, and 56.8[b]
Lateral length	Horizontal	m			367.5		361.7
	Along center-line	m			367.87		362.1
Support tower height		m			3.8		3.7
Maximum in-span elevation differentials		m			1.2		0.65, 1.15, and 1.50[c]
Lateral diameter		mm	127			127.0/76.2/ 50.8[d]	162.3/136.4/101.6[e]
Absolute roughness	Lateral pipe	mm			0.005		0.0015
	Drop-tube	mm			0.0015		0.0015
Drop-tube length range		m			3.05-4.25		2.59-4.38
Constant above ground clearance of sprinkler-*prv* assembly		m			0.75		0.76
Drop-tube diameter		mm			19.05		
Field surface slope		%	0.0	-1.5	1.5	0.0	-1.7/0.0
Local head loss Parameters	branching, outlet	-			0.04		0.03
	line-flow, outlet	-			0.01		0.008
	bending, connector	-			0.05		0.02
	span joints	-			0.06		0.04
	reduction[f]	-	-			0.29/0.248[g]	0.104/0.195[h]
Total head at the inlet[i]		m			30		23.4 and 27.7
Elev. at the inlet		m	3.8	10.3	3.85	3.8	4.84

[a]Data-sets 1 to 3 consider alternative hydraulic scenarios in which the same lateral is operated on fields with different slopes. Data-set 4 shares the same parameter set with data-set 1, except lateral diameter.

[b]In data-sets 5 and 6, effective span lengths, i.e., lengths used for modeling purposes, vary. It is 50.8 m for span 1, 56.8 m for spans 2 to 6, and is 27 m for span 7.

[c]The maximum in-span elevation differential for data-sets 5 and 6 vary: it is 1.5 m for the upstream-end span, 1.15 m for spans 2 to 6 each, and is 0.65 m during irrigation for span 7.

[d]Lateral diameter is 127 mm over spans 1 to 4, it is then reduced to 76.2 mm in span 5, and to 50.8 mm in span 6.

[e]Pipe diameter of 163.3 mm was used over spans 1 to 6. It is then reduced to 136.4 mm over the upper 13.8 m section of span 7, which is further reduced to 101.6 mm in the lower 13.2 m long reach of the span.

[f]The local head loss coefficients for lateral diameter reductions are obtained from Granger based on pipe diameter ratios.

[g]0.29 and 0.248 are for the diameter reductions at the inlet end of spans 5 and 6, respectively.

[h]0.104 and 0.195 are for the diameter reductions at the inlet end and midpoint of span 7, respectively.

[i]The inlet head for data-sets 1 to 4 is 30 m and those of data-sets 5 and 6 are 23.4 and 27.7 m, respectively.

Table 1: Lateral hydraulic, geometric and elevation data used in hydraulic simulations.

Lateral parameters		**Units**	**Data-sets**	
			1 to 4	**5 and 6**
Number of *prvs*, sprinklers, and drop-tubes		-	289	349
Sprinkler model is Super spray UP3, the nozzle sizes are		*mm (in)*	3.572 (9/64)	4.763 (3/16)
Sprinkler pressure-discharge function	ρ	$L/s/m^{\lambda}$	0.0429	0.0771
	λ	-	0.5018	0.4998
Sprinkler spacing, horizontal		*m*	1.25	0.58-1.65
prv model is PSR2	h_{prv}	*m*	6	4.2
	δh_{prv}	*m*	3.5	3.5
	h_{max}	*m*	90	90

Note: ρ and λ are coefficient and exponent, respectively, of the sprinkler head-discharge function and are derived through regression from the data provided in manufacturer's catalogue. h_{prv} is *prv*-set pressure head; δh_{prv} is the minimum required pressure head margin, between the *prv*- inlet pressure and h_{prv}, in order for the *prv* to operate reliably in the active mode; and h_{max} is the maximum allowable pressure at the *prv* inlet for the *prv* to operate in the active mode.

Table 2: Sprinkler and prv data used in hydraulic simulations.

in Table 2. The model of the *prv* used in the linear-move system is PSR2 and is manufactured by Senninger [16]. The *prv*-set pressure, the maximum allowable inlet pressure for the *prv* to operate reliably in the active mode, and the minimum required pressure head margin between the inlet pressure and the set pressure for the *prv* to operate reliably in the active mode are summarized in Table 2.

Data-sets 2 and 3: In order to assess the effects of contrasting field slopes on lateral pressure variability patterns, data-sets 2 and 3 consider alternative hydraulic scenarios in which exactly the same lateral as that of data-set 1 is operated in fields with constant slopes of -1.5 and 1.5%, respectively (Table 1). The total head imposed at the inlet of the lateral is 30 m, which is the same as that of data-set 1. The lateral inlet elevations for data-sets 2 and 3 are 10.3 and 3.85 m, respectively, with respect to a datum consisting of a surface that contains the point on the lateral with the lowest elevation.

As noted earlier, the elevation profile of each span of data-set 1 is symmetric about the point of maximum in-span elevation, which overlaps with the span mid-point. In data-sets 2 and 3, however, the negative/positive field slopes introduced asymmetry in the elevation profile of the lateral with respect to the point of maximum in-span elevation. As a result, for each span of data-set 2 for instance, the upstream span section within which elevation increases with distance from the lateral inlet is 25 m and the corresponding rise in elevation is only 0.78 m. On the other hand, the total decrement in elevation in each span of data-set 2, which occurs over the lower 36.25 m section of the span is 1.7 m. By contrast, for data-set 3, the span section over which lateral elevation increases with distance from inlet is 36.25 m and the corresponding increment in elevation is 1.7 m. The total decrement in the in-span elevation is 0.78 m and occurs over the lower 25 m reach of the spans. As will be shown shortly, the elevation profile asymmetry, introduced by the negative/positive field slopes, will have significant effects on the spatial pattern of the pressure head profiles of these laterals.

Note that the elevation profiles of the spans of data-sets 2 and 3 were computed from that of data-set 1 by simply rotating the field surfaces, and hence the spans, through vertical angles of -0.015 rad and 0.015 rad, respectively, relative to a level surface. Note that such a purely geometric approach to estimating the elevation profiles of linear-move systems that run on sloping fields, does not take into account the effects of local adjustments that may occur near the flexible span joints of the lateral as field slope is varied.

Data-set 4: Data-set 4 shares the same lateral hydraulic, geometric, and elevation profile characteristics with that of data-set 1, except for lateral diameter. Data-set 1 considers a lateral with a constant diameter of 127 mm over all its spans. Data-set 4, on the other hand, uses a diameter of 127 mm over spans 1 to 4, which is then reduced to 76.2 mm in span 5, and to 50.8 mm in span 6 (Table 1). Note that data-set 4 is included here to illustrate the effects of variations in lateral diameter on pressure head variability patterns of linear-move laterals.

Data-sets 5 and 6: Data-sets 5 and 6 represent a pair of irrigation events in which an actual lateral is operated in the same field under two different total inlet heads. Hence, these data-sets share the same parameter set except the total head at the lateral inlet, which is set to 23.4 m for data-sets 5 and is equal to 27.7 m for data-set 6 (Table 1). Detailed discussion on system components and the geometric, hydraulic, and elevation profile characteristics of the lateral are provided by Zerihun et al. [11]. Thus, only a concise description is presented here.

The lateral has six full spans, each supported at both ends, and a seventh span at the distal-end, which consists of a beam supported only at its upstream-end. The full length of span 1 is 54.8 m, although the effective span length considered for modeling purposes is 50.8 m. Each of spans 2 to 6 are 56.8 m in length. Spans 1 to 6 have concave profile, thus in each span the point of maximum in-span elevation occurs somewhere between the inlet and distal-ends of the span and the point of minimum in-span elevation occurs at either end or both ends of the span. The setting of span 1 is such that it is inclined at a slope of -1.7% over its effective length. Mainly because of the negative slope, the elevation profile of span 1 is nonsymmetric about a vertical line through the point of maximum in-span elevation. Thus, the span section over which elevation increases with distance from the lateral inlet is 15.7 m long and the total rise in elevation over this section is only 0.3 m. On the other hand, the total decrement in elevation, which occurs over the lower 35.1 m long segment of the span, is 1.5 m.

In contrast to span 1, spans 2 to 6 operate on a level field and the elevation profile of each of these spans can be considered symmetric about the span's mid-point. Thus, the total rise and fall in elevation over each of these spans is the same and is equal to 1.15 m. The elevation of the upstream-end of the lateral section considered here for modeling purposes is 4.89 m and is measured with respect to the level field surface.

The distal-end span of the lateral is only 27 m long (Table 1). The span is operated on a level field and its centerline consists of a convex curve that is asymmetric with respect to the point of minimum in-span elevation. Over the upper 13.8 m long section of the span, elevation decreased by a total of 0.25 m to the in-span minimum of 3.35 m and the span elevation then rose to the in-span maximum of 4.0 m over the lower 13.2 m reach of the span. Note that the elevation profile of the distal-end span varies depending on whether the system is operational (i.e., applying irrigation and hence carrying water) or is idling and has been emptied. The elevation profile data of the distal-end span highlighted here corresponds to a scenario in which the system is operational. The elevation profile of the concave spans (i.e., spans 1 to 6) was modelled with the equation of an ellipse and that of the distal-end span was described in terms of a cubic polynomial.

The lateral diameter over spans 1 through 6 is 162.3 mm. Lateral diameter is then reduced to 136.4 mm over the upper 13.8 m section of span 7 and is further reduced to 101.6 mm over the lower 13.2 m reach of the span. Drop-tube lengths, which vary between 2.59 and 4.38 m, were set such that each *prv*-sprinkler assembly was suspended from a lateral outlet at a uniform above ground clearance of about 0.76 m (2.5 ft), if the lateral was to be operated on a level field [17]. The drop-tubes have a diameter of 19.05 mm (3/4″). An absolute roughness of 0.0015 mm was used for both the lateral pipes and the drop-tubes.

Sprinkler spacing varies along the lateral between 0.58 and 1.65 m. The sprinkler model used in data-sets 5 and 6 is the same as that of data-sets 1 to 4. However, the sprinkler nozzle size used in data-sets 5 and 6 is 4.763 mm (3/16") compared to the 3.572 mm (9/64") used in data-sets 1 to 4. The *prv* used in data-sets 5 and 6 is of the same model and has the same settings as those of data-sets 1 to 4. The hydraulic characteristics of the sprinkler and the *prvs* used in this system are summarized in Table 2.

Comparison of the equation with a numerical model

For each of data-sets 1 to 6, the pressure profiles computed with Eqn. 13 and those obtained through hydraulic simulations are depicted in Figures 6a-6f. Each of the charts in Figure 6 shows four different curves. These include the pressure profile computed with Eqn. 13 depicted as circles, the simulated lateral pressure profile shown in

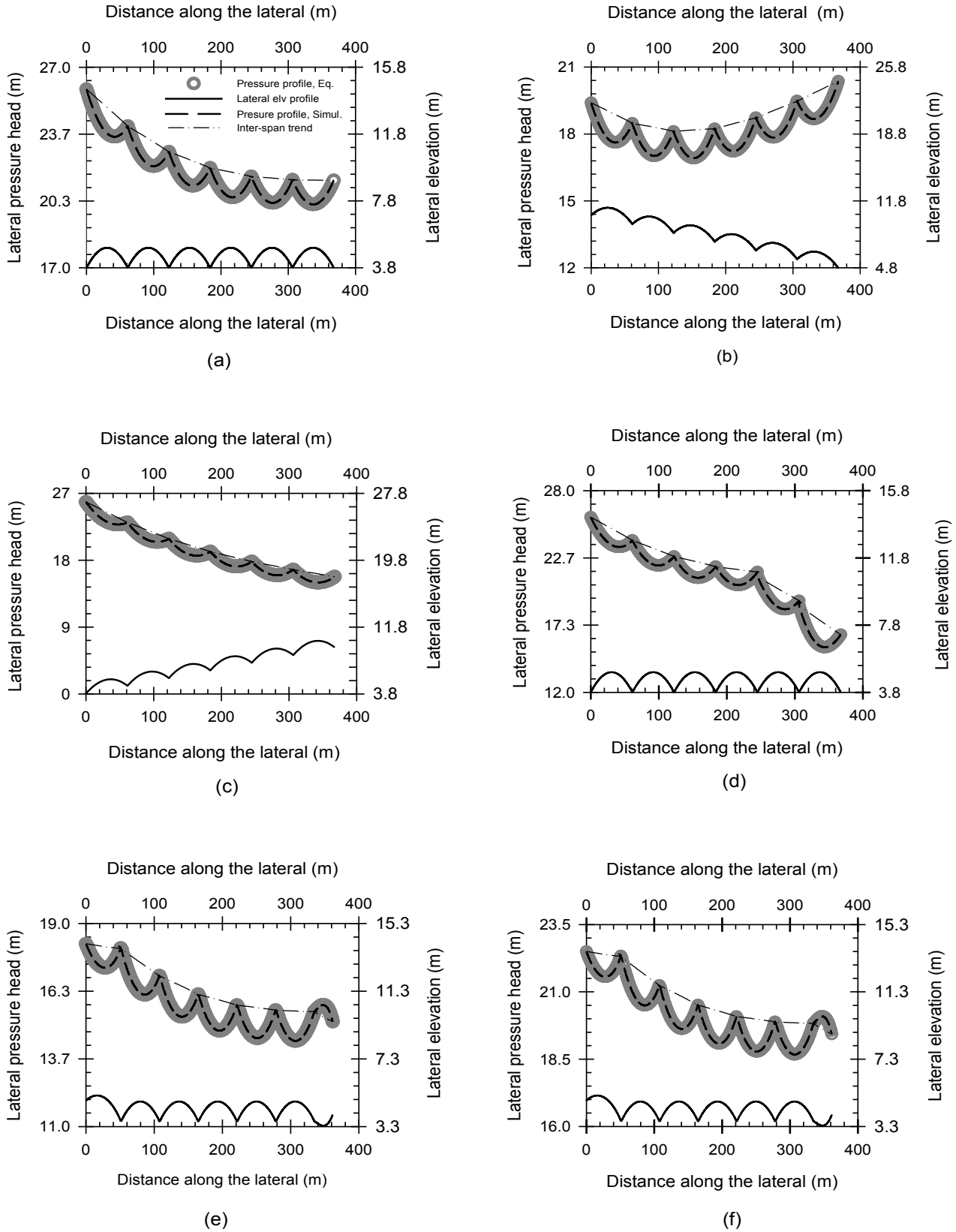

Figure 6: Comparison of simulated lateral pressure profiles with those obtained based on equation: (a) data-set 1, (b) data-set 2, (c) data-set 3, and (d) data-set 4, (e) data-set 5, and (f) data-set 6.

Data-set #	Absolute residuals (%)		
	Minimum	Maximum	Average
1	0.0078	0.0100	0.0093
2	0.0093	0.0112	0.0106
3	0.0103	0.0178	0.0144
4	0.0066	0.0109	0.0083
5	0.0073	0.0092	0.0085
6	0.0082	0.0566	0.0141
Overall minimum	0.0066		
Overall maximum		0.0566	
Overall average			0.0109

Table 3: Absolute residuals between pressure profiles computed with the model and obtained with equation.

dashed line, the elevation profile of the lateral centerline in solid line, and a curve showing the inter-span lateral pressure variability trends as a dash-dot line. Descriptions of the inter-span pressure variability trends will be provided shortly.

Overall, visual indications suggest that the lateral pressure head profiles computed with Eqn. 13 closely match those obtained through simulation (Figures 6a-6f). To obtain a quantitative measure of the differences between the pressure predictions of Eqn. 13 and the lateral hydraulic model, a simple error metric termed as the percent relative residuals or simply absolute residuals is introduced here. Accordingly, the percent relative residuals of lateral pressure head profiles are defined as the absolute differences between the lateral pressure heads computed with the equation and the model, expressed as percentage of those computed with the model.

For each data-set, the resultant minimum, maximum, and average percent residuals of lateral pressure head profiles are summarized in Table 3. The percent relative residuals, between the lateral pressure heads computed with Eqn. 13 and the hydraulic model, vary between a minimum of 0.0066% obtained for data-set 4 and a maximum of 0.0566% for data-set 5. The average percent residuals of the lateral pressure head profiles range from 0.0083% for data-set 4 to 0.0144% for data-set 3 and the overall average residual of the pressure heads is 0.0109%. Results of the evaluation suggest that the pressure profiles computed with Eqn. 13 closely match those obtained through simulations, lending additional support to the validity of the pressure profile patterns of linear-move laterals reported by Zerihun et al. [11].

Discussion on lateral pressure head profile patterns

In contrast to the rather smooth pressure profiles of solid-set and set-move irrigation system laterals, the pressure profiles of linear-move laterals exhibit a distinctly wavy pattern (Figures 6a-6f). As a result, two different forms of spatial variability attributes, consisting of local span-scale variability patterns (shown as dashed lines or circles) and a broader inter-span/lateral-wide trends (depicted as dotted lines) can be discerned in the pressure head profiles of these laterals. Thus, a complete description of the lateral pressure head profile patterns of linear-move systems may require that both spatial variability attributes be assessed.

In-span lateral pressure variability attribute: As can be noted from Figures 6a-6f, the local span-scale (in-span) pressure head profile variability patterns exhibit some general attributes that are repeated, although with some variation, along a linear-move lateral. It can be observed that for the concave spans the corresponding local in-span lateral pressure head variability patterns invariably follow a convex form, consisting of an upstream section over which pressure decreases with distance from the lateral inlet to a local minimum somewhere within the span and a downstream section over which pressure increases with distance from the lateral inlet. The total span-scale decrement in pressure, which occurs over an upstream section of a concave span where pressure is a decreasing function of distance from the lateral inlet, will henceforth be referred to as the in-span pressure loss. On the other hand, the total rise in pressure from the span-minimum, which occurs over a downstream section of a concave span where pressure is an increasing function of distance from the lateral inlet, will be referred to as the in-span pressure recovery (gain).

While spans of linear-move laterals generally have a concave form, a cantilever type distal-end span characterized by a convex elevation profile is used in systems where the dimension of the irrigated field justifies it (Figures 6e and 6f). Note that for both data-sets 5 and 6, the in-span pressure variability patterns corresponding to the convex span exhibit a concave form. Thus, the lateral pressure profiles show increasing trends over an upstream section of the convex span, followed by a decreasing trend in a lower section of the span.

The preceding implies that the characteristic forms of the in-span pressure variability patterns of linear-move laterals, at a minimum, include convex and concave curves. Physical reasoning suggests that the in-span pressure variability patterns observed here are generally related to the geometry of the spans. A closer look at Figure 6 shows that for a lateral consisting of identical spans, the specifics of the in-span lateral pressure variability attributes (such as the magnitudes of the in-span pressure gains relative to the corresponding in-span pressure losses) vary from span to span along the lateral. It will now be shown that this variation in net in-span pressure gain/loss along a lateral gives rise to the inter-span/lateral-wide variability trends, noted above. In addition, simulation results will be used to show that inter-span pressure variability trends are modulated not only by the span geometry, but also by other parameters including the slope of the field in which a lateral is installed.

The inter-span lateral pressure variability attribute: The pressure differentials across individual spans, when considered over two or more consecutive spans, yields a trend in pressure variability over multiple spans. Such a pressure variability attribute is referred here as the inter-span lateral pressure variability trend. The actual pressure profiles of linear-move laterals exhibit relatively complex spatial variability attributes. As a result, the broader inter-span/lateral-wide trends inherent in such a profile may not be readily discernible. Thus, a simpler curve obtained by connecting the pressure heads at the inlet- and distal-ends of each span is used here, instead of the actual pressure profile, to represent the inter-span/lateral-wide pressure variability trend along a lateral, which is shown in each of Figure 6a-6f as a dash-dot line. The goal is to use the readily discernible and distinct monotonic properties of such a curve to characterize the overall spatial variability attributes of pressure over an entire lateral or a section of it encompassing two or more consecutive spans.

Data-sets 1, 2, and 3: As can be noted from the data description section, data-sets 1, 2, and 3 represent alternative hydraulic scenarios in which exactly the same lateral is operated in fields with 0, -1.5, and 1.5% slopes, respectively. It can be observed from Figures 6a and 6c that when the lateral is operated in a level field (data-set 1) or in a field with a constant positive slope (data-set 3) each of the resultant inter-span pressure variability curves exhibit a decreasing trend along the lateral, but at a decreasing rate. By comparison, operating the same lateral in a field with a negative slope (data-set 2) resulted in an inter-span pressure variability curve with two segments (Figure 6b),

consisting of an upstream segment where the curve trends down as one moves downstream along the lateral and a downstream segment over which the curve tends upwards. Given that these data-sets differ only in the slope of the fields in which the lateral is operated, it can be noted that the differences in the broader lateral pressure profile patterns of these data sets can be attributed entirely to the differences in the corresponding lateral elevation profiles.

Remarkably, the inter-span pressure variability trends shown in Figures 6a-6c, for data-sets 1, 2, and 3, respectively, are analogous in form to pressure profile patterns that would have been obtained if a solid-set or set-move irrigation system lateral is operated in fields with similar slopes [14]. This suggests that the inter-span pressure variability trend curves, with their distinct monotonic property, were able to capture the effects of field slope on the broader lateral-wide pressure variability trends in a manner that is readily discernible, compared to the actual pressure profiles. The inter-span pressure variability curves can be particularly useful if, for instance, a graphical comparison of the effects of alternative field slopes on the overall lateral-wide pressure variability trends is to be made. They would result in clear and uncluttered charts compared to charts obtained based on the actual pressure profiles.

Data-set 4: The inter-span pressure variability curve of data-set 4 generally tends downwards as one moves downstream along the lateral. However, it is comprised of two sections with distinctly different rates (Figure 6d). The first part covers spans 1 to 4, where the inter-span pressure variability curve is trending downwards along the lateral, but at a decreasing rate. Over spans 5 and 6, on the other hand, the inter-span pressure variability curve continues to trend downwards as one moves downstream along the lateral, but at more rapid rate than is observed in the spans immediately upstream. As a result, the inter-span pressure variability trend over spans 5 and 6 exhibits a departure from the overall trend observed over the upstream spans.

As noted in the data description, data-set 4 considers a lateral with variable diameter. A diameter of 127 mm is used over spans 1 to 4, which is then reduced to 76.2 mm in span 5 and to 50.8 mm over span 6. The rapid pace with which the inter-span pressure variability curve declined over spans 5 and 6 compared to spans immediately upstream is related to the significant and progressive reduction in lateral diameter over spans 5 and 6. The reductions in lateral diameter have led to significant increases in friction head losses in these spans. A closer look at the model outputs show that friction head losses, in spans 5 and 6, are about five to six time greater than that of span 4, respectively. The output data also shows that the tapering lateral diameter have led to increases in local head losses and velocity heads, in spans 5 and 6, compared to span 4. The combined effect is relatively large drops in pressure over these spans compared to the spans immediately upstream, which explains the rapid rate with which the inter-span pressure variability trend curve declined over spans 5 and 6 in contrast to the spans immediately upstream.

Note that the relative simplicity of the inter-span pressure variability curves, compared to the actual lateral pressure profiles, makes them particularly convenient in graphical comparisons of the effects of alternative lateral diameters and field slopes on the broader lateral-wide trends of the pressure profiles of linear-move systems.

Data-set 5: Data-set 5 is based on an irrigation event in which an actual lateral with six full spans and a seventh distal-end span, consisting of a truncated cantilever type beam, is used to irrigate a level field. Figure 6e shows that the inter-span pressure variability curve of data-set 5 is generally trending downwards as one moves downstream along the lateral. However, a closer look at the curve shows that distinctly different trends can be discerned along the lateral. A section of the inter-span pressure variability curve, that covers span 1, has a significantly shallower slope than the section encompassing the spans immediately downstream. The inter-span pressure variability curve also has a steeper slope over span 7 compared to sections of the curve covering the upstream spans.

The relatively shallower slope of the inter-span pressure variability curve, in span 1, is mainly related to the steep negative slope (-1.7%) that the span is set on (Table 1). The relatively steep negative slope led to an asymmetry in the elevation profile of the span (Figure 6e). It can be noted from the data description section that the total in-span decrement in elevation, which occurred over a lower section of the span, is five times larger than the total in-span increment in elevation that occurred in an upper section of the span. This resulted in a significant gain in pressure in the lower section of the span compared to the in-span pressure loss in the upper section of the span. Hence, the resultant net in-span pressure loss is significantly smaller in span 1 compared to spans located immediately downstream, which explains the relatively shallower slope of the inter-span pressure variability curve over this span.

Spans 2 to 6 consist of identical spans that have near symmetrical elevation profile patterns about their mid-points and are operated on a level field. Over these spans the inter-span pressure variability trends downwards, but at a decreasing rate as one moves downstream along the lateral (Figure 6e). Note that this observation is consistent with the inter-span trend obtained for data-set 1, where a series of identical concave spans with a symmetric elevation profile pattern about their mid-points are operated on a level field.

The relatively larger span-scale decline in pressure across span 7 compared to spans upstream is related to the effects of reduced pipe diameter and in-span elevation profile asymmetry. As can be noted from the data description section, a diameter of 162.3 mm is used in spans 1 to 6. Lateral diameter is then reduced to 136.4 mm over the upper half of span 7 and then to 101.6 mm over the lower half of the span. Although span 7 is installed on a level surface, the convex curve representing the centerline of the span is nonsymmetric with respect to the point of minimum in-span elevation. As a result, the total span-scale rise in elevation, which occurs in the lower section of the span, is about two and half times greater than the total in-span decrement in elevation which occurs over the upper section of the span. The combined effect of reduced pipe diameter and in-span elevation asymmetry has led to a relatively large net in-span pressure loss, which explains the steep slope of the inter-span pressure variability curve over span 7 compared to the spans upstream.

Data-set 6: Data-sets 5 and 6 represent two irrigation events in which an actual lateral is operated in the same field under different inlet heads: 23.4 m for data-set 5 and 27.7 m for data-set 6. While the pressure profiles of data-sets 5 and 6 (Figures 6e and 6f) are different, overall the inter-span lateral pressure variability trends obtained for both data-sets are similar. Descriptions of the broader inter-span pressure variability trend provided above for data-set 5, therefore, apply to that of data-set 6 as well. Hence, no separate discussion will be given here on the inter-span pressure variability trend of data-set 6.

Note that sections of the inter-span pressure variability trend curves, straddling concave spans, invariably appear at the top of the actual pressure profiles (Figures 6a-6f). By contrast, segments of the

lateral-wide pressure variability curves covering the convex span (Figures 6e and 6f) are located at the bottom of the pressure profile. Note that this is related to the convexity structure of the respective in-span pressure variability patterns.

Discussion and Conclusion

An equation that relates lateral pressure explicitly with distance from the lateral inlet is derived for linear-move sprinkler irrigation laterals. The equation takes into account the effects of both span geometry and field slope on lateral elevation profile and hence lateral pressure. The explicit pressure-distance equation is derived from its more general form (obtained based the energy conservation principle for one-dimensional steady flow in pipes) through analysis of the spatial behaviors of each of the parameters that affect lateral pressure.

The proposed lateral pressure profile equation is not intended for predictive use. Instead, pressure profiles computed with the equation are used here in an additional evaluation of the validity of the distinct pressure head profile patterns of linear-move laterals produced, in an earlier study, through numerical simulations. Accordingly, pressure profiles of linear-move laterals computed with the equations were compared with those obtained based on hydraulic simulations. Six data-sets covering a range of lateral parameters and field slopes were used in the evaluation. The maximum residual between the pressure head profiles computed with the equation and those obtained through simulations is 0.0566% of the simulated pressure heads and the overall average residual is 0.0109%. The results show that estimates of lateral pressure profiles computed with the equation closely match those obtained through hydraulic simulations, lending additional support to the validity of the unique spatial patterns of linear-move laterals reported in an earlier study.

Overall, pressure head profiles computed with the equation proposed here confirm an observation made in an earlier study that the spatial variability characteristics of the pressure profile of a linear-move lateral exhibit dual characteristics, consisting of local in-span variability patterns and a broader inter-span/lateral-wide trend. Hence, a complete description of the spatial variability attributes of pressure along these laterals may require that both the in-span and inter-span trends be assessed.

Specifically, the results of the current study show that pressure profiles of linear-move laterals are comprised of a series of convex and at times concave curves. The convex in-span pressure variability patterns were invariably observed over spans that have a concave form. By comparison, concave in-span lateral pressure variability patterns were observed over a span with a convex elevation profile. Furthermore, it was shown that span-scale pressure differentials, when considered over multiple consecutive spans, yield an inter-span/lateral-wide pressure variability trend. The inter-span/lateral-wide pressure variability trend along a lateral is represented here in terms of a simple curve (with readily discernible monotonic characteristics) produced by connecting the pressure heads at the inlet- and distal-ends of each span. Results show that the inter-span pressure variability trend curve, defined as such, effectively captures the broader lateral-wide variability attributes of pressure in a way that is not only readily discernible, but also suitable for comparison and analysis of alternative hydraulic scenarios.

Furthermore, a function that relates pressure slope with lateral slope and friction slope is deduced here from the pressure head profile equation. The pressure slope equation can be used in the analysis and characterization of the full range of variation of the pressure profile patterns of laterals. However, the current analysis is limited to highlighting some important properties of the equation.

Analysis of the spatial behaviors of key lateral hydraulic parameters and elevation profiles, conducted as part the derivation of the pressure equation, has revealed some interesting properties of the parameters and lateral pressure profile itself. An important result stemming from this analysis relates to the observation that lateral pressure head profile is a piecewise linear function of distance from the lateral inlet with discontinuities at the computational nodes. As a result, lateral pressure profiles are defined not at the computational nodes, but about the computational nodes. The practical implication of this result is that a more complete description of a lateral pressure profile takes the form of an array in which pressure about each computational node is defined in terms of a pair of values, consisting of pressure heads computed at a point just upstream and another one at a point just downstream of the node. The inlet and distal-end nodes are, however, exceptions. For these nodes pressure needs to be defined only in terms of a single value each.

References

1. Kincaid DC, Heermann DF (1970) Pressure Distribution on a Center-Pivot Sprinkler Irrigation System. Trans ASAE, 13(5):556-558.
2. Chu ST, Moe DL (1972) Hydraulics of a Center Pivot System. Trans ASAE, 15(5):894-896.
3. Keller J, Bliesner R (1990) Sprinkle and trickle irrigation. Van Nostrand Reinhold, New York, NY.
4. Scaloppi EJ, Allen RG (1993) Hydraulics of Center-Pivot Laterals. J Irrig Drain Eng ASCE, 119(3): 554-567.
5. Fraisse CW, Heermann DF, Duke HR (1995) Simulation of Variable Water Application with Linear-Move Irrigation System. Transactions of the ASAE, 38(5):1371-1376.
6. Anwar AA (1999) Friction Correction Factors for Center-Pivots. J Irrig Drain Eng ASCE, 125(5): 280-286.
7. Valiantzas JD, Dercas N (2005) Hydraulic Analysis of Multidiameter Center-Pivot Sprinkler Laterals. J Irrig Drain Eng ASCE, 131(2): 137-142.
8. Heermann DF, Stahl KM (2006) CPED: Center Pivot Evaluation and Design. Center for Agricultural Resources Research, Water Management and Systems Research, USDA-ARS, Fort Collins, CO.
9. Tabuada MA (2014) Friction Head Loss in Center-Pivot Laterals with Single Diameter and Multidiameter. J Irrig Drain Eng ASCE 140(10): 04014033.
10. Zerihun D, Sanchez CA (2019) Hydraulics of Linear-Move Sprinkler Irrigation Systems, II: Model Development. Irrig Drain Sys Eng 8(2): 236.
11. Zerihun D, Sanchez CA, Thorp KR, Hagler MJ (2019) Hydraulics of linear-move sprinkler irrigation systems, III: Model evaluation. Irrig Drain Sys Eng 8(2): 237.
12. Martin DL, Heermann DF, Madison M (2007) Design and Operation of Farm Irrigation Systems. Chapter 15. Hydraulics of Sprinkler and Micro-Irrigation Systems. Hoffmans GJ, Evans RG, Jensen ME, Martin DL, Elliott RL, eds. 2nd Ed. ASABE St. Joseph, MI, 532-555.
13. Zerihun D, Sanchez CA, Bautista E (2019) Slope Effects on the pressure Head profile Patterns of Sprinkler Irrigation Laterals, I. Theoretical Analysis. Irrig Drain Systems Eng, 7(3):221.
14. Zerihun D, Sanchez CA, Bautista E (2019) Slope Effects on the pressure Head profile Patterns of Sprinkler Irrigation Laterals, II. Evaluation Based on Simulation. Irrig Drain Systems Eng, 7(3):222.
15. Senniger (2017) Super Spray: Customizable Field Proven Technology, Agricultural Irrigation, Low Pressure- High Performance.
16. Senninger (2017) Pressure Regulator Guide, Agricultural, Residential & Commercial Irrigation, Low Pressure-High Performance.
17. Senninger (2015) Chart No. MK-923-13B. Senninger Irrigation Inc., Clermont, Florida.